# **Uncovering Model Processing Strategies with Non-Negative Per-Example Fisher Factorization**

## Michael Matena <sup>1</sup> Colin Raffel <sup>2</sup>

## **Abstract**

We introduce NPEFF (Non-Negative Per-Example Fisher Factorization), an interpretability method that aims to uncover strategies used by a model to generate its predictions. NPEFF decomposes per-example Fisher matrices using a novel decomposition algorithm that learns a set of components represented by learned rank-1 positive semi-definite matrices. Through a combination of human evaluation and automated analysis, we demonstrate that these NPEFF components correspond to model processing strategies for a variety of language models and text processing tasks. We further show how to construct parameter perturbations from NPEFF components to selectively disrupt a given component's role in the model's processing. Along with conducting extensive ablation studies, we include experiments to show how NPEFF can be used to analyze and mitigate collateral effects of unlearning and use NPEFF to study in-context learning. Furthermore, we demonstrate the advantages of NPEFF over baselines such as gradient clustering and using sparse autoencoders for dictionary learning over model activations.

## 1. Introduction

Interpretability methods in machine learning aim to understand how models process examples and form their predictions. A recent thread of interpretability research has focused on decomposing internal model activations to uncover monosemantic interpretable components that be used to help reason about the predictions and behavior of the model (Bricken et al., 2023). In this work, we propose an analysis method called NPEFF (non-negative per-example Fisher factorization) that operates instead on on *parameter space representations* to provide complementary insights.

Namely, NPEFF components correspond to strategies and heuristics used by the model in its processing rather than features present in the activations.

We represent each example using what we call its perexample Fisher (PEF) matrix, a positive semi-definite (PSD) matrix that relates perturbations in parameter space to changes in the model's predictive distribution. The directions in parameter space associated with each of the model's computational substeps thus become imprinted in its PEFs. Decomposing sets of PEFs can therefore uncover groups of commonly used substeps which we call model processing strategies. We introduce a novel decomposition algorithm that approximates PEFs as a non-negative combination of components represented by rank-1 PSD matrices. These components can then be used to construct perturbations of the model parameters to selectively disrupt their associated processing strategies.

After introducing methods to make working with PEFs tractable, we run NPEFF analysis on a variety of language models and tasks. We then explore properties of these decompositions through automated and human analysis, run extensive ablation studies, and compare to potential baseline methods. We finally demonstrate applications of NPEFF in the analysis of unlearning and in-context learning (ICL). We release our code to facilitate the use of NPEFF and to aid in further research.

Our key contributions can be summarized as:

- We introduce PEFs as an object characterizing the model's per-example processing along with mathematical and software tools to enable working them.
- 2. We introduce a novel decomposition algorithm that recovers common processing from a group of PEFs.
- 3. We introduce a principled method to selectively disrupt specific processing strategies.

## 2. Methods

#### 2.1. Collection of PEFs

Consider the conditional distribution  $p_{\theta}(y|\mathbf{x})$  of a model parameterized by  $\theta \in \mathbb{R}^n$  given an example  $\mathbf{x}$ . We define the

<sup>&</sup>lt;sup>1</sup>Department of Computer Science, University of North Carolina at Chapel Hill <sup>2</sup>Vector Institute, University of Toronto. Correspondence to: Michael Matena <matema@cs.unc.edu>.

per-example Fisher (Fisher, 1922), or PEF, as the positive semidefinite (PSD)  $n \times n$ -matrix

$$F(\mathbf{x}) = \mathbb{E}_{y \sim p_{\theta}(y|\mathbf{x})} \nabla_{\theta} \log p_{\theta}(y|\mathbf{x}) \nabla_{\theta} \log p_{\theta}(y|\mathbf{x})^{T}. \quad (1)$$

The PEF allows us to relate small perturbations  $\delta \in \mathbb{R}^n$  in the model parameters to changes in the model's predictive distribution  $p_{\theta}(y|\mathbf{x})$  via (Amari, 2016):

$$D_{\mathrm{KL}}(p_{\theta}(y|\mathbf{x})||p_{\theta+\delta}(y|\mathbf{x})) \approx \frac{1}{2}\delta^{T}F(\mathbf{x})\delta.$$
 (2)

For a typical classification model,  $p_{\theta}(y|\mathbf{x})$  corresponds to a categorical distribution over class labels. In this work, we additionally consider language models, which predict a sequence of token IDs from a vocabulary of tokens conditioned on a prefix,  $p_{\theta}(y|\mathbf{x})$  can be a distribution over a set of potential endings to a prefix, a subset of the vocabulary, or the entire vocabulary. We consider any of these options to effectively define a set of possible predictions and continue to treat  $p_{\theta}(y|\mathbf{x})$  as a categorical distribution (though we will consider a series of approximations to make calculation of the expectation in Equation (1) tractable in Section 2.1.2). Letting r denote the number of categories, we can exactly represent the PEF using an  $r \times n$ -matrix  $G(\mathbf{x})$ as  $F(\mathbf{x}) = G(\mathbf{x})^T G(\mathbf{x})$  where the *i*-th row of  $G(\mathbf{x})$  is equal to  $\sqrt{p_{\theta}(y_i|\mathbf{x})}\nabla_{\theta}\log p_{\theta}(y_i|\mathbf{x})$ . We call  $G(\mathbf{x})$  the low-rank matrix representation of the PEF, or the LRM-PEF.

## 2.1.1. RANDOM PROJECTIONS

To make storing LRM-PEFs across a data set tractable, we apply a sparse random projection (Li et al., 2006) to the rows of  $G(\mathbf{x})$ . Random projections are a dimensionality reduction procedure that approximately preserves inner products between vectors. We developed a custom CUDA kernel that computes these projections efficiently without needing to materialize the projection matrix. See Appendix A for details.

## 2.1.2. APPROXIMATING THE EXPECTATION

While we can conceptually consider the distribution over the set of possible continuations produced by a language model as a categorical distribution, handling the expectation over y in (1) exactly is infeasible due to the large number of options. While we could approximate the expectation by sampling multiple  $y \sim p_{\theta}(y|\mathbf{x})$ , we instead opt for a method based on random projections. This method allows for the PEF to capture information across the whole distribution rather than just a few options.

Let  $\mathbf{q}(\mathbf{x}; \theta) \in \mathbb{R}^r$  be defined element-wise with its i-th entry equal to  $\mathtt{stop\_grad}(\sqrt{p_{\theta}(y_i|\mathbf{x})})\log p_{\theta}(y_i|\mathbf{x})$ , where  $\mathtt{stop\_grad}$  treats a quantity as a constant while backpropagating. If  $A \in \mathbb{R}^{r' \times r}$  is a random projection matrix (i.e.

 $A^T A \approx I$ ), then  $\nabla_{\theta} A \mathbf{q}(\mathbf{x}; \theta) \in \mathbb{R}^{r' \times n}$  works well as a stand-in for the LRM-PEF  $G(\mathbf{x}) = \nabla_{\theta} \mathbf{q}(\mathbf{x}; \theta) \in \mathbb{R}^{r \times n}$ . See Appendix B for a proof.

#### 2.1.3. RANK REDUCTION

While the LRM-PEF representation is exact, we can construct a lower-rank *approximation* to the PEF using SVD to further reduce its storage costs. Notably, we can apply SVD after the random projection step, which greatly reduces its computational cost. See Appendix C for more details. This approximation works especially well when the singular values of the PEF matrix decay rapidly.

## 2.2. Decomposition

Given a set  $G_1, \ldots, G_m$  of LRM-PEFs over a set of m examples and a number C of components to learn, we define NPEFF as a non-negative factorization expressed as the nonconvex optimization problem

minimize 
$$\sum_{i=1}^{m} \|G_i^T G_i - \sum_{j=1}^{C} W_{ij} \mathbf{h}_j \mathbf{h}_j^T \|_F^2$$
 subject to 
$$W_{ij} \geq 0.$$
 (3)

In words, NPEFF aims to find a set of C rank-1 PSD matrices  $\mathbf{h}_j \mathbf{h}_j^T$  and a set of non-negative coefficients  $W_{ij}$  for each PEF that produces a good reconstruction. We call the vector  $\mathbf{h}_j$  corresponding to a component its pseudo-Fisher vector.

Details of how we solve (3) can be found in Appendix D. As a high level overview, we alternate between updating the coefficients  $W_{ij}$  and updating the pseudo-Fisher vectors  $\mathbf{h}_j$ . The coefficient update is similar to a multiplicative update step in non-negative matrix factorization (Lee & Seung, 1999). The pseudo-Fisher update step is a gradient descent step. Notably, our implementation directly operates on the low-rank representations and does not require materializing any full PSD matrices.

We found it important for training stability to initialize the pseudo-Fisher vectors by performing only the pseudo-Fisher vector update step at the start of training. Furthermore, we normalize each PEF  $G_i^TG_i$  to unit Frobenius norm to prevent examples with large norm PEFs from dominating the loss. Following completion of the decomposition, we typically normalize each component's rank-1 matrix to unit Frobenius norm and rescale the coefficients accordingly. This puts coefficients across components on the same scale. We finally note that given the pseudo-Fisher vectors of a decomposition, we can fit coefficients to an arbitrary set of PEF by only performing the coefficient update step repeatedly.

#### 2.2.1. Interaction with Random Projections

In Appendix D.6, we demonstrate that the optimization problem (3) and our algorithm is still meaningful when operating on randomly projected PEFs. We show that using projected PEFs should lead to approximately the same coefficients and pseudo-Fisher vectors that are approximately projections of what would have been learned.

One drawback of operating on projected PEFs, however, is that the pseudo-Fisher vectors  $\mathbf{h}_j$  belong to the projected space rather than the original parameter space. Parameter-space pseudo-Fisher vectors can be useful for confirming that NPEFF components do correspond to processing strategies used by the model. For example, consider perturbing the model parameters in the direction of the pseudo-Fisher vector. Following the information geometric interpretation (2) of PEF matrices, this should preferentially affect the model's predictions on examples with a large coefficient for that component.

When a vector is sparse, it can be possible to "reverse" a random projection and recover the projected vector from its projection via compressed sensing (Donoho, 2006). We have good reason to expect parameter-space pseudo-Fisher vectors to be sparse because the overparameterization of models leads to gradients with respect many of the parameters being consistently insignificant (Frankle & Carbin, 2018). Since the pseudo-Fisher vector corresponds to the subset of parameters responsible for a particular processing strategy implemented by the model, we can expect them to be even sparser.

We make use of the compressed sensing algorithm introduced in Hale et al. (2007). This algorithm only requires matrix-vector products with the random projection matrix and its transpose, which our custom CUDA kernels efficiently support. We leave development of more bespoke parameter-space pseudo-Fisher recovery algorithms to future work.

## 3. Experiments

## 3.1. Characterizing Component Tunings

**Setup** As a first view of NPEFF's utility, we ran NPEFF on a representative group of models and tasks to explore the components it produced. We focus on language models and natural language tasks, but we expect that NPEFF would be effective in other modalities as well. For a classification model, we used a variant of BERT-base (Devlin, 2018) fine-tuned on the natural language inference task MNLI (Williams et al., 2018) and evaluate on SNLI (Bowman et al., 2015). For autoregressive language models, we used the 135M, 360M, and 1.7B parameter versions of SmolLM2 (Allal et al., 2024) on the sentiment analysis

task SST2 (Socher et al., 2013) and question answering task TriviaQA (Joshi et al., 2017), respectively. These represent tasks where  $p_{\theta}(y|\mathbf{x})$  ranges over a subset of the vocabulary and the entire vocabulary, respectively. We use a zero-shot formulation for the language models. See Appendix E for more information on the formulation of these tasks and how we constructed  $p_{\theta}(y|\mathbf{x})$  for them.

For SNLI and SST2, we used 500,000 and 60,000 examples respectively, a projected dimension of 8192 and 16,192 respectively, and 8192 and 512 components respectively. For TriviaQA, we used 133,838 examples, a projected dimension of 8192, approximated the expectation using 16 projections, SVD reduced the PEF rank to 4, and used 2048 components. We ignore the embedding and LayerNorm parameters when computing the PEFs. For all NPEFF decompositions, we used a warm-up of 1000 frozen coefficient steps with a learning rate of 1e-5 and another 3000 steps with a learning rate of 3e-4.

**Top component examples** Following existing work on interpretability methods that use sparse autoencoders to decompose activations (Rajamanoharan et al., 2024), we begin to get a qualitative sense for a component's tuning by looking at the examples with the highest coefficient for each component. Top examples from a component selected from each of our decompositions are presented in Figure 1. Top examples from random components can be found in Appendix J.

**Validating component tooling** Apart from manually inspecting top examples, we hope to obtain a more quantitative picture of component tuning. Since SNLI and SST2 had a fixed set of classes as labels, we can perform an automated analysis by labeling a component as tuned if more than 95% of its top 16 examples had the same label as its ground truth / prediction. For TriviaQA, such automated analyis is not possible, and we therefore resorted to human evaluation. For human analysis, we created groups of examples that were either the top examples for a component or random examples (control). Evaluators were asked to answer yes/maybe/no if the examples had a common theme and write a short description of the theme if present. Each group was seen by 2 different evaluators. We note, however, that evaluation of interpretability methods remains an open research problem (Gao et al., 2024). In particular, we note that our evaluation methods here should be used to simply verify that component top examples generally have properties consistent with our expectations.

Our results are presented in Table 1. For SNLI and SST2, a significant proportion of components were tuned to predictions or labels. Most TriviaQA component top examples had a detectable theme, determined by a yes or maybe label, with only a few false positives on the control groups. The

## SNLI

- [P] The child in the blue shirt is running through the sand.
- [H] The child's shirt is black.
- [P] A man wearing a blue shirt and baseball cap is tied to a pole
- [H] The shirt is black
- [P] A man wearing a blue shirt sitting on a wall smoking
- [H] The shirt is red.
- [P] A guy wearing and blue shirt on his knee taking a picture.
- [H] The man is wearing a grey shirt

#### SST2

- a low-budget affair
- a low-rent retread of the alien
- a low-budget affair, tadpole
- , low-budget and tired

#### TRIVIAQA

In which year did Mozart die?

In which year did General Franco die?

In which year did Elvis die?

In which year did Beethoven die?

Figure 1. Top examples of selected components from NPEFF decompositions in Section 3.1.

Table 1. Tuning information in percentages.

SNLI		SS	ST2	TriviaQA		
PRED	Label	PRED	Label	TOP	CONTROL	
75.7	47.6	56.1	39.2	79	3	

inter-evaluator agreement in our human evaluations on TriviaQA was 86%. Overall, these results indicate that NPEFF component top examples have properties that are consistent with representing model processing strategies.

## **3.2.** Component Tunings on Held-Out Examples

As discussed in Section 2.2, we can fit NPEFF coefficients to arbitrary PEFs given learned pseudo-Fisher vectors. Under the hypothesis that NPEFF uncovers genuine model processing strategies, component tunings should remain similar when gleaned from held-out examples.

We ran experiments to confirm this using set-ups similar to SNLI, SST2, and TriviaQA from Section 3.1 using fewer examples to compute the decomposition to leave held-out examples from each dataset. We also reduced the number of components to reflect the smaller number of examples. For SNLI/SST/TriviaQA, we used 250,000/30,000/70,000 held-in examples respectively, 250,000/30,000/53,838 held-out examples respectively, and 4096/256/1024 components respectively.

To determine whether component tunings were consistent between the held-in and held-out examples, we adapted the evaluation methods from Section 3.1 to compare the top examples from the held-in set to the top examples from the held-out set. Specifically, for SNLI and SST2 we used an automated analysis where we determined whether components on the held-in set tuned to a prediction or ground truth label had the same tuning on the held-out set. For TriviaQA, we used a human analysis where human evaluators were presented with a pair of groups of examples. They were then asked to answer yes/maybe/no if the two pairs of groups

*Table 2.* Percentages of components with the same tuning across held-in and held-out sets.

SI	SNLI		ST2	TRIVIAQA		
Pred	Label	PRED LABEL		SAME	DIFF	
92.6	70.0	86.0	81.8	78	15	

had a similar theme amongst their examples. The pairs either were top examples from the same component but from different sets of examples or they were the top examples of different components from the held-in set to act as controls. Each pair was seen by 2 different evaluators.

We present our evaluation results in Table 2. For SNLI and SST2, most of the components with tunings on the held-in set had the same tuning on the held-out set. We found no components that had inconsistent tunings on both the held-in and held-out set. Hence, these percentages are not 100% most likely due to imprecision in our automatic tuning detection. For TriviaQA, most pairs of top examples from the component were deemed to have the same theme, determined by a yes or maybe label, with relatively few false positives on pairs of top examples from different components. The inter-evaluator agreement was 73%.

#### 3.3. Perturbations

Following the method described in Section 2.2.1, we can design perturbations using compressed sensing to reconstruct pseudo-Fisher vectors in parameter space from their projections. While using the pseudo-Fisher vector directly works well, we can improve the selectivity by orthogonally rejecting it from the other pseudo-Fisher vectors. This arises from wanting a perturbation orthogonal to all pseudo-Fisher vectors other than the one we want to affect. In practice, we found that only rejecting from vectors with an absolute cosine similarity less than a threshold worked best. These steps can be performed using the projected vectors.

To evaluate the perturbed model, we first compute the av-

*Table 3.* Perturbation results, where the values are the geometric mean across components.

MODEL	TASK	KL-RATIO	NORM RATIO
BERT-BASE-NLI	SNLI	18.59	0.072
SMOLLM2-135M	SST2	10.94	1.02

erage KL-divergence of the perturbed model's predictions from the original model's predictions on a per-example basis. To normalize these values, we report the ratio of the mean KL-divergence for the component's top examples to the mean KL-divergence over a set of random examples. We report the ratios of the average PEF norms for these groups to represent how relatively sensitive top examples are to perturbations (1). Since the rank-1 PSD matrix corresponding to a Fisher pseudo-vector is invariant under multiplying the vector by -1, we try perturbations in both directions and report the higher KL-ratio.

We ran perturbations experiments using the SNLI and SST2 decompositions from Section 3.1 for 256 and 128 randomly selected components, respectively. We used a similarity threshold of 0.5 for orthogonal rejection, used 16 component top examples, and a random set of 1,000 baseline examples. We used a perturbation L2 magnitude of 3e1 for SNLI and 2e1 for SST2. Results are summarized in Table 3 with more experimental details presented in Appendix F. The the predictions of the perturbed models were significantly more different on component top examples than the baseline examples, indicating that the processing strategies associated with the components were selectively disrupted. Since the PEF norm ratios are far smaller than the KL-divergence ratios, our results cannot be explained by component examples being generally more sensitive to perturbations.

## 4. Ablations

We explored the impact of various hyperparameters of the PEF computation and NPEFF decomposition on the resultant components. Except where mentioned otherwise, the experimental settings were taken from Section 3.1.

#### 4.1. Random Projection Size

We tried using random projection sizes of 128, 1024, 8192, and 32,768 for BERT-base on SNLI. Note that the 128 and 1024 sizes used a dense projection matrix since our implementation was significantly faster in those cases. We used 100,000 examples and 1024 NPEFF components.

To create a similarity metric between a pair of NPEFF decompositions, we started with the cosine similarity of a pair of component coefficient vectors to compare components. We found that components with a high cosine similarity tended to have similar top examples and tunings. For each component in one decomposition, we take the maximum cosine similarity with a component in the other decomposition. If this value is high for every component in both decomposition, then each component has a corresponding similar component in the other decomposition. We take the mean of this max cosine similarity across all components in the decompositions to get a single score.

The NPEFF with projected dimension of 128 had similarity score of around 0.4 across all of the 1024, 8192, and 32,768 dimension NPEFFs. The NPEFF with projected dimension of 1024 had a similarity score of around 0.75 with both the 8192 and 32,768 dimension NPEFFs. The NPEFF with projected dimension of 8192 had a similarity score of 0.82 with the 32,768 dimension NPEFF. These similarity scores indicate that the decompositions with a projected dimension of 1024 or greater had quite similar components. The extremely small projected dimension of 128 led to a greater change in the resultant NPEFF components; however, the similarity score still indicates that the decompositions were substantially similar.

### 4.2. Number of Components

We ran experiments varying the number of NPEFF components using set-ups similar to SNLI and SST2 from Section 3.1. For SNLI, we tried using 128, 512, and 2048 components. For SST2, we tried using 32, 64, 128, 256, and 512 components.

We found that components tend to "split" as the number of components increase: Essentially, a component tuned to a general processing strategy gets converted to multiple components tuned to more specific instantiations of that general strategy. To map a component to its corresponding splits from another decomposition, we use the cosine similarity of component coefficient vectors to compare components between decompositions. For each component in the fine-grained decomposition, we find the component in the coarse-grained decomposition with the largest similarity score. This creates a map from each coarse-grained component to its set of corresponding fine-grained splits.

When running this identification, we find that all or almost all of the coarse-grained components have at least one matching fine-grained component amongst pairs of decompositions. Note that we would expect coarse-grained components tuned to a model prediction to have their prediction tuning preserved in their fine-grained splits since they represent more specific instantiations of a general processing strategy. For each pair of decompositions, we restrict our analysis to coarse-grained components with at least 95% of their top 16 examples having the same predicted label. We then count the number of their fine-grained matches with the same prediction tuning and divide by their total number

*Table 4.* Decomposition similarity scores to the full EPS rank decomposition within each row.

	SVD RANK								
EPS	1	2	4	8	16	32			
64	0.75	0.83	0.87	0.90	0.91	0.94			
16	0.75	0.82	0.87	0.90 0.89					
4	0.74	0.84							

of matches to get the fraction of tunings preserved. We get values of 86.9% for SNLI and 76.1% for SST2 averaged across all pairs of decompositions, which indicates that tunings tend to carry over from the coarse-grained components to their splits. A full breakdown in provided in Appendix G.

## 4.3. Expectation Approximation and SVD Rank Reduction

Recall that to efficiently compute the expectation in Equation (1) when the space of possible outputs is large, we introduced a strategy using random projections. To experiment with the effect of this projection step, we ran experiments using SmolLM2-360M on TriviaQA using 1, 4, 16, and 64 expectation projections. Further, recall that as discussed in Section 2.1.3, we use SVD to reduce the rank of the PEFs to reduce computational costs. To study the impact of using the SVD, we explore ranks of 1, 2, 4, 8, 16, 32, and 64, where applicable. We used a random projection size of 8192, used 40,000 examples, and 256 NPEFF components. We again use the similarity score from Section 4.1 to compare decompositions.

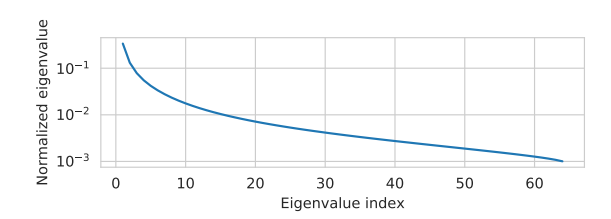


Figure 2. Log-scale plot of the mean decay of normalized eigenvalues of PEF matrices with 64 expectation random projections.

Results for varying the SVD-reduced rank while holding the expectation projection size (EPS) fixed are provided in Table 4. Each row contains the similarity score to the decomposition with the SVD rank set to the EPS. We see that even reducing the rank to 1 results in a fairly similar decomposition with larger ranks. We present a log-scale plot of the mean decay of normalized eigenvalues for the PEFs with expectation projection size 64 in Figure 2. Since the eigenvalues drop off quickly, we conclude that the SVD rank reduction can retain much of the information contained

in the PEFs.

We also study the effects of varying the EPS while setting the SVD rank to the EPS. When compared to the EPS 64 decomposition, using an EPS of 1 produces a similarity score of 0.51, an EPS of 4 produces a similarity score of 0.66, and an EPS of 16 produces a similarity score of 0.79. This suggests that while using more projections in the expectation captures more information, even using a single projection can produce fairly similar decompositions. We leave further improvements, such as varying the number of projections used based on the entropy of the model's predictive distribution, to future work.

#### 5. Baselines

## 5.1. Gradient Clustering

Gradient clustering, as presented in (Michaud et al., 2024; Marks et al., 2024), starts by computing the gradient of the loss for each example, making use of random projections for dimensionality reduction. These gradients are normalized to unit L2 norm and then clustered using k-means. Since NPEFF does not make use of ground-truth labels, we slightly modify this formulation by taking the gradient of  $\log p_{\theta}(y'|\mathbf{x})$ , where  $y' = \operatorname{argmax} p_{\theta}(y|\mathbf{x})$ . Since (Michaud et al., 2024) only took gradients where the model correctly predicted the next token with low entropy, these formulations coincide reasonably closely to their set-up.

One disadvantage of this baseline is that gradients of the log probability of a single class capture less information about the model's predictive distribution than PEFs (which compute gradients with respect to all possible predictions), especially for high entropy distributions. Another disadvantage comes from each example being assigned to a single cluster. This precludes clusters from decomposing the model's processing vertically into common substeps. Furthermore, it cannot adequately represent situations where the model's predictions for an example arise from a superposition of multiple independent processing strategies.

To demonstrate the problems with using gradients instead of PEFs, we ran an experiment using SmolLM2-360M on TriviaQA. We computed gradients for 80,000 examples that were projected to a dimension of 32,768. K-means clustering was performed on those gradients to get 2048 clusters. Recall that the model's predictive distribution ranges over all 49,152 elements of vocabulary in this set-up. This distribution had a mean entropy of 4.43 nats with almost every example having an entropy over the threshold of 0.1 nats used in (Michaud et al., 2024). Using proximity to the cluster centroid to rank examples within a cluster, we found that 1690 out of 2048 clusters had all of their 16 top examples share the same  $\arg\max p_{\theta}(y|\mathbf{x})$ . In contrast, only 384 out of 2048 NPEFF components from Section 3.1 had this

Table 5. Percentage of SAE components with given tunings.

	Layer 2	Layer 5	Layer 8	Layer 11
LABEL	0.26	1.00	2.19	3.70
Pred	0.20	0.70	2.47	4.92
TOKENS	41.3	40.3	22.5	7.75

same property. This demonstrates that PEFs capture more information from the model's entire predictive distribution while need to choose a single class for gradients can bias the decomposition.

### **5.2.** Activation Sparse Autoencoders

Activation sparse autoencoders come from mechanistic interpretability research (Bricken et al., 2023), which aims to better understand models by precisely understanding their underlying processing. Based on the hypothesis that raw model activations are a superposition of sparsely activated monosemantic concepts, activation sparse autoencoders to uncover those concepts using sparse dictionary learning. We make use of the TopK-SAE from Gao et al. (2024), which makes of a TopK function in the encoder to explicitly make latent activations sparse.

To exemplify the differences between activation SAEs and NPEFF, we ran experiments on the NLI fine-tuned BERTbase using SNLI as the dataset. We learned SAEs for activations taken from the inputs to the attention sub-layer on the 2nd, 5th, 8th, and 11th layers of this 12 layer model. All of our SAEs had a latent dimension of 8192, and we experimented with sparsities of k = 16, 32, 64, 128. To evaluate SAE tunings, we took the examples with the 16 highest coefficient values for each SAE component. Components with non-zero coefficients on fewer than 16 examples were deemed "dead" and discarded. Given these component top examples, tuning to the ground truth and predicted labels was determined as in Section 3.1. We also deemed a SAE component as tuned to a particular group of tokens if greater than 95% of its top examples had a non-zero coefficient on the same set of tokens. Full information about the SAE training and evaluation can be found in Appendix H.1.

Results for the fraction of non-dead SAE components with detected tunings are presented in Table 5. We found these results to be similar across the sparsities k, so the average is presented there. A full breakdown can be found in Appendix H.2. Generally, more SAE components became tuned to labels and predictions at higher layers while the fraction of components tuned token groups decreased at higher levels. Nevertheless, fewer than 5% of SAE components were tuned to labels or predictions even at layer 11 while 47.6% and 75.7% of NPEFF components were tuned to labels and predictions, respectively, in our 8192

component decomposition from Section 3.1.

Generally, we found activation SAEs to provide a view into the model internals complementary to that provided by NPEFF. SAE components tend to be tuned to fine-grained features of the examples while NPEFF components tend to be tuned to common model processing strategies. Using activations SAEs to reconstruct explicit circuits corresponding to the model processing strategies uncovered by NPEFF is a promising line of future research (Marks et al., 2024).

## 6. Applications

### 6.1. Unlearning

Unlearning aims to change the model's predictions on a set of examples while leaving its predictions on the rest of the examples relatively unchanged. To perform unlearning, we use a variant of gradient ascent (Yao et al., 2023) that is detailed in Appendix I.1. At a high level, the examples to forget are put in what is called the forget set while the rest of the examples are deemed the retain set. Unlearning proceeds by optimizing a loss that aims to increase the KL-divergence of the unlearned model's predictions from the original model's predictions on the forget set and keep the KL-divergence small on the retain set.

While we only perform gradient ascent on the forget set explicitly, unlearning will have some deleterious effects on the model's processing of other examples. Since NPEFF components correspond to model processing strategies, we hypothesize that NPEFF components with a large coefficient on the forget set will tend to have their processing disrupted. We further hypothesize that we can mitigate this disruption by over-representing such examples in the retain set.

For our experimental setting, we chose SmolLM2-360M on TriviaQA. Here, components were often tuned to particular types of questions such as asking what year different people died (Figure 1). If we wanted the model to forget the year a specific person died, for example, then we would want the unlearning to not affect the model's responses on the component's other top examples.

We performed unlearning runs for 64 different components where we took the component's top example as the forget set. For each component, we selected the next 24 examples with the highest coefficient, which we randomly divided into two sets of 12 examples each. One of these sets is set aside to be used to evaluate the impact of the unlearning, which we call the top examples evaluation set. The other set is appended to each batch in the retain set in the mitigation set-up. In control experiments, we append 12 randomly selected examples to each batch in the retain set instead. Full details are presented in Appendix I.2.

We used the KL-divergence of the unlearned model's pre-

Table 6. KL-divergence values (nats) of unlearned models evaluated on different sets.

	Forget	TOP EXAMPLES	RANDOM
MITIGATION	136.4	1.42	7.87E-2
CONTROL	141.1	3.71	7.53E-2

dictive distribution with the original model's predictive distribution to measure the unlearning's disruption on a perexample basis. All of the control experiments produced a KL-divergence greater than 10 nats on the forget set while 16 of the mitigation experiments failed to do so. This indicates that overrepresenting similar examples in the retain set can lead to difficulties in unlearning. We restrict the rest of our analysis to the experiments operating on the 48 other forget set examples.

Our results are presented in Table 6. The forget column is the KL-divergence of the forget set example. The top examples column is the median KL-divergence for the top examples evaluation set. The random column in the median KL-divergence for a random set of 10,000 examples. All values are averaged across runs. It is clear that the processing corresponding to the forget example's NPEFF component is disrupted by the unlearning procedure. The other component top examples have their processing disrupted significantly more than random examples. Furthermore, our mitigation procedure significantly reduces the impact on those examples.

#### 6.2. ICL

ICL involves including a prefix consisting of labeled examples when prompting a language model to perform a task. Some work has suggested that models often do not learn the rules of the task *per se* but rather learn the how the task is structured from the examples in the context (Min et al., 2022). Interestingly for zero-shot SmolLM2-135M on SST2, we found that while many components were tuned to ground truth labels and the model's predictions, the ground truth and predicted label were often different. This indicates that the model's ability to distinguish between the classes is not being fully reflected in its predictions, further supporting a claim from Min et al. (2022).

Based on this, we constructed a classifier based on zero-shot NPEFF component tunings. We first found the components where at least 75% of the top examples were tuned to a particular ground truth label. Then, we constructed a matrix with shape n\_classes × n\_components with ones in locations corresponding to tuned components and zeros elsewhere. We multiply an example's NPEFF coefficient vector by this matrix to get scores for each class and take the highest score as the prediction. This provides a weighted

score of the label-tuned processing strategies used on the example.

For our 512 component decomposition, this classifier obtains an accuracy of 87.6% compared to 66.1% for the zero-shot model. To compare to ICL, we found a 6 example context as the best of 50 random contexts evaluated on a subset of 1024 examples (Zhang et al., 2022), which had an accuracy of 87.5% across the entire dataset. Our NPEFF-based classifier agreed with the ICL model on 87.6% examples compared to an agreement of 68.9% with the zero-shot model. These results indicate that, at least in this scenario, much of the gains from ICL come from adapting to the specific presentation of the task rather than the model learning new processing strategies from the context.

## 7. Related Work

While our use of *per-example* Fisher matrices is novel, variants of Fisher information matrices have been explored in the contexts of optimization (Martens, 2020), continual learning (Kirkpatrick et al., 2017), and model merging (Matena & Raffel, 2022; Tam et al., 2023). Methods to efficiently represent these matrices include a diagonal approximation (Kirkpatrick et al., 2017) and a Kronecker-factorized representation (Martens & Grosse, 2015).

The line of mechanistic interpretability involving SAEs also relies on unsupervised decompositions to extract interpretable components (Cunningham et al., 2023; Gao et al., 2024; Bricken et al., 2023). These methods rely on variants of sparse dictionary learning (Olshausen & Field, 1996). By contrast, NPEFF's decomposition algorithm can be seen as a extension of NMF (Lee & Seung, 1999) that follows from positive semi-definiteness taking the place of non-negativity.

(Michaud et al., 2024) use gradient clustering to discover what they call skill and knowledge "quanta", which is roughly equivalent to our model processing strategies, in a language modeling task. (Marks et al., 2024) improved the scaling of this method by performing clustering on random projections of gradients. Both papers, however, restricted their analysis to cases where the model correctly predicted the next token with low entropy.

## 8. Conclusion

NPEFF presents a novel method to understand what strategies a model uses to process examples. We introduced PEFs as a novel object to characterize a model's processing of an example along with tools to make working with them tractable. We examined properties of NPEFF components and demonstrated how to selectively disrupt their associated processing strategies. In addition to conducting extensive ablation studies, we used NPEFF to analyze unlearning

and ICL. Furthermore, we demonstrated the advantages of NPEFF over baselines including gradient clustering and activation SAEs. In future work, we hope to explore the use of NPEFF in the context of mechanistic interpretability as complementary to use of activation SAEs.

## **Impact Statement**

This paper presents work whose goal is to advance the field of Machine Learning. There are many potential societal consequences of our work, none which we feel must be specifically highlighted here.

## References

- Allal, L. B., Lozhkov, A., Bakouch, E., Blázquez, G. M., Tunstall, L., Piqueres, A., Marafioti, A., Zakka, C., von Werra, L., and Wolf, T. Smollm2 with great data, comes great performance, 2024.
- Amari, S.-i. *Information geometry and its applications*, volume 194. Springer, 2016.
- Bowman, S. R., Angeli, G., Potts, C., and Manning, C. D. The snli corpus. 2015.
- Bricken, T., Templeton, A., Batson, J., Chen, B., Jermyn, A., Conerly, T., Turner, N., Anil, C., Denison, C., Askell, A., et al. Towards monosemanticity: Decomposing language models with dictionary learning. *Transformer Circuits Thread*, 2, 2023.
- Burred, J. J. Detailed derivation of multiplicative update rules for nmf. *Paris, France*, 2014.
- Cunningham, H., Ewart, A., Riggs, L., Huben, R., and Sharkey, L. Sparse autoencoders find highly interpretable features in language models. *arXiv preprint arXiv:2309.08600*, 2023.
- Devlin, J. Bert: Pre-training of deep bidirectional transformers for language understanding. *arXiv* preprint *arXiv*:1810.04805, 2018.
- Donoho, D. L. Compressed sensing. *IEEE Transactions on information theory*, 52(4):1289–1306, 2006.
- Fisher, R. A. On the mathematical foundations of theoretical statistics. *Philosophical transactions of the Royal Society of London. Series A, containing papers of a mathematical or physical character*, 222(594-604):309–368, 1922.
- Frankle, J. and Carbin, M. The lottery ticket hypothesis: Finding sparse, trainable neural networks. *arXiv* preprint *arXiv*:1803.03635, 2018.

- Gao, L., la Tour, T. D., Tillman, H., Goh, G., Troll, R., Radford, A., Sutskever, I., Leike, J., and Wu, J. Scaling and evaluating sparse autoencoders. *arXiv preprint arXiv:2406.04093*, 2024.
- Hale, E. T., Yin, W., and Zhang, Y. A fixed-point continuation method for 11-regularized minimization with applications to compressed sensing. *CAAM TR07-07, Rice University*, 43(44):2, 2007.
- Joshi, M., Choi, E., Weld, D., and Zettlemoyer, L. triviaqa: A Large Scale Distantly Supervised Challenge Dataset for Reading Comprehension. arXiv e-prints, art. arXiv:1705.03551, 2017.
- Kirkpatrick, J., Pascanu, R., Rabinowitz, N., Veness, J., Desjardins, G., Rusu, A. A., Milan, K., Quan, J., Ramalho, T., Grabska-Barwinska, A., et al. Overcoming catastrophic forgetting in neural networks. *Proceedings of the national academy of sciences*, 114(13):3521–3526, 2017.
- Lee, D. D. and Seung, H. S. Learning the parts of objects by non-negative matrix factorization. *nature*, 401(6755): 788–791, 1999.
- Li, P., Hastie, T. J., and Church, K. W. Very sparse random projections. In *Proceedings of the 12th ACM SIGKDD international conference on Knowledge discovery and data mining*, pp. 287–296, 2006.
- Marks, S., Rager, C., Michaud, E. J., Belinkov, Y., Bau, D., and Mueller, A. Sparse feature circuits: Discovering and editing interpretable causal graphs in language models. *arXiv* preprint arXiv:2403.19647, 2024.
- Martens, J. New insights and perspectives on the natural gradient method. *Journal of Machine Learning Research*, 21(146):1–76, 2020.
- Martens, J. and Grosse, R. Optimizing neural networks with kronecker-factored approximate curvature. In *International conference on machine learning*, pp. 2408–2417. PMLR, 2015.
- Matena, M. S. and Raffel, C. A. Merging models with fisher-weighted averaging. *Advances in Neural Information Processing Systems*, 35:17703–17716, 2022.
- Michaud, E., Liu, Z., Girit, U., and Tegmark, M. The quantization model of neural scaling. *Advances in Neural Information Processing Systems*, 36, 2024.
- Min, S., Lyu, X., Holtzman, A., Artetxe, M., Lewis, M., Hajishirzi, H., and Zettlemoyer, L. Rethinking the role of demonstrations: What makes in-context learning work?, 2022. URL https://arxiv.org/abs/2202.12837.

- Olshausen, B. A. and Field, D. J. Emergence of simple-cell receptive field properties by learning a sparse code for natural images. *Nature*, 381(6583):607–609, 1996.
- Rajamanoharan, S., Conmy, A., Smith, L., Lieberum, T., Varma, V., Kramár, J., Shah, R., and Nanda, N. Improving dictionary learning with gated sparse autoencoders. arXiv preprint arXiv:2404.16014, 2024.
- Socher, R., Perelygin, A., Wu, J., Chuang, J., Manning, C. D., Ng, A., and Potts, C. Recursive deep models for semantic compositionality over a sentiment treebank. In *Proceedings of the 2013 Conference on Empirical Methods in Natural Language Processing*, pp. 1631–1642, Seattle, Washington, USA, October 2013. Association for Computational Linguistics. URL https://www.aclweb.org/anthology/D13-1170.
- Tam, D., Bansal, M., and Raffel, C. Merging by matching models in task subspaces. arXiv preprint arXiv:2312.04339, 2023.
- Williams, A., Nangia, N., and Bowman, S. A broad-coverage challenge corpus for sentence understanding through inference. In *Proceedings of the 2018 Conference of the North American Chapter of the Association for Computational Linguistics: Human Language Technologies, Volume 1 (Long Papers)*, pp. 1112–1122. Association for Computational Linguistics, 2018. URL http://aclweb.org/anthology/N18-1101.
- Yao, Y., Xu, X., and Liu, Y. Large language model unlearning. *arXiv preprint arXiv:2310.10683*, 2023.
- Zhang, Y., Feng, S., and Tan, C. Active example selection for in-context learning. *arXiv preprint arXiv:2211.04486*, 2022.

## A. Random Projections

Random projection matrix form To project from  $\mathbb{R}^n$  to  $\mathbb{R}^r$ , let  $A \in \mathbb{R}^{n \times r}$  be a random projection matrix. For computational purposes, we want most entries of A to be zero. To do this, let  $\mathbf{a} \in \mathbb{R}^n$  denote a column of A. We pick a region size  $s \in \mathbb{N}$  and divide the entries of  $\mathbf{a}$  into chunks of size s. In each of these chunks, we pick an entry at random and set it with equal probability to either 1 or -1. All other entries are 0. Following Marks et al. (2024), we pick a level of sparsity such that each entry of the original vector will, on average, contribute to 32 entries in its projection. This corresponds to selecting a sparse region size of s = r/32.

Efficient projections using a CUDA kernel Note that explicitly materializing even a sparse representation of the projection matrix would take 32n values, i.e. 32 times the number of model parameters. However, we can construct entries of the matrix on the fly using a pseudo-random number generator. Hence the seed of the pseudo-random number generator essentially parameterizes the projection matrix.

This is a good fit to implement the projection via a CUDA kernel. In our current implementation, each thread in the kernel corresponds to one of the r entries in the projection. The global seed specifying the projection matrix is used to produce a different seed for each thread. This pseudo-random number generator is then used to select the entry from each sparse region and its value.

## **B. Expectation Approximation Proof**

Let us start by restating the expressions from Section 2.1.2. Let  $\mathbf{q}(\mathbf{x};\theta) \in \mathbb{R}^r$  be defined element-wise with its i-th entry equal to  $\mathtt{stop\_grad}(\sqrt{p_{\theta}(y_i|\mathbf{x})})\log p_{\theta}(y_i|\mathbf{x})$ , where  $\mathtt{stop\_grad}$  treats a quantity as a constant while backpropagating. Note that  $\nabla_{\theta}\mathbf{q}(\mathbf{x};\theta) = G(\mathbf{x}) \in \mathbb{R}^{r \times n}$  is the LRM-PEF.

Let  $A \in \mathbb{R}^{r' \times r}$  be a random projection matrix (i.e.  $A^T A \approx I$ ). Let  $G'(\mathbf{x}) = \nabla_{\theta} A \mathbf{q}(\mathbf{x}; \theta) \in \mathbb{R}^{r' \times n}$  be our approximation to the LRM-PEF. We have  $G'(\mathbf{x}) = \nabla_{\theta} A \mathbf{q}(\mathbf{x}; \theta) = A \nabla_{\theta} \mathbf{q}(\mathbf{x}; \theta) = AG(\mathbf{x})$ . When construct the full PEF, when have  $F'(\mathbf{x}) = G'(\mathbf{x})^T G'(\mathbf{x}) = G(\mathbf{x})A^T AG(\mathbf{x}) \approx G(\mathbf{x})IG(\mathbf{x})^T = G(\mathbf{x})G(\mathbf{x})^T = F(\mathbf{x})$ . Hence our use of this random projection to approximate the expectation results in a similar PEF to representing the full expectation.

## C. SVD Rank Reduction

Consider an LRM-PEF  $G \in \mathbb{R}^{r \times n}$ . The corresponding PEF matrix will be  $F = G^T G \in \mathbb{R}^{n \times n}$ . Let r' < r be the rank that we want to reduce the PEF to. Consider the SVD  $G = U \Sigma V^T$ . Let  $\Sigma \in \mathbb{R}^{r' \times r'}$  and  $V' \in \mathbb{R}^{n \times r'}$  be the submatrices corresponding to the top r' singular values. The reduced rank LRM-PEF is given by  $G' = \Sigma' V'^T$ . We can ignore the U matrix since it is orthogonal and thus  $U^T U = I$ , so it does not affect the transformation from the LRM-PEF to the PEF matrix.

## D. Decomposition Algorithm

We start by reviewing the optimization problem from Section 2.2. Given a set  $G_1, \ldots, G_m$  of LRM-PEFs over a set of m examples and a number C of components to learn, NPEFF can be expressed as the non-convex optimization problem

minimize 
$$\sum_{i=1}^{m} \|G_i^T G_i - \sum_{j=1}^{C} W_{ij} \mathbf{h}_j \mathbf{h}_j^T \|_F^2$$
 subject to 
$$W_{ij} \ge 0.$$
 (4)

We stack the PEFs into a single rank-3 tensor  $G \in \mathbb{R}^{m \times r \times n}$ . We can express the quantities to be learned via the matrices  $W \in \mathbb{R}^{m \times C}$  and  $H \in \mathbb{R}^{C \times n}$ , where rows of H correspond to the  $\mathbf{h}_j$ . Our optimization of (4) proceeds in alternating steps of updating the coefficients W and pseudo-Fishers W. Our W-update step is essentially a the W-update step from the multiplicative update NMF (Lee & Seung, 1999). algorithm. For the W-update step, we perform a gradient descent step with a fixed learning rate.

## D.1. W-Update Step

Recall that the multiplicative update step in NMF involves computing non-negative numerator and denominator matrices  $N, D \in \mathbb{R}^{m \times C}$ . The matrix W is then updated via the element-wise rule  $W_{ij} \mapsto W_{ij} N_{ij} / D_{ij}$ .

Computing the numerator starts with computing the rank-3 tensor  $B \in \mathbb{R}^{m \times r \times C}$ , where r is the rank used to represent the LRM-PEFs, with elements given by  $B_{ijk} = \sum_{\ell=1}^n G_{ij\ell} H_{k\ell}$ . The numerator is then given element-wise by  $N_{ik} = \sum_{j=1}^r B_{ijk}^2$ . The denominator is then given by  $D = W((HH^T) \odot (HH^T))$ , where  $\odot$  denotes the Hadamard product.

## D.2. H-Update Step

The gradient of the loss with respect to H consists of two terms  $T_1, T_2 \in \mathbb{R}^{C \times n}$  that are added together. The first term is given by  $T_1 = 4((W^TW) \odot (HH^T))H$ . Computation of the second term starts by computing the rank-3 tensor  $B \in \mathbb{R}^{m \times r \times C}$  as was done for the W-update step. The second term is then obtained element-wise as  $[T_2]_{i\ell} = -4\sum_{j=1}^m \sum_{k=1}^r W_{ji}B_{jki}G_{jk\ell}$ .

## **D.3. Multi-GPU Implementation Details**

To speed up decompositions and support larger decompositions, we implement a multi-GPU strategy for our algorithm. We partition the input PEFs and the coefficients W along the batch dimension across separate GPUs. We replicate the pseudo-Fisher matrix H on each GPU. The W-update step can proceed on each GPU without the need for inter-GPU communication. Since the gradient of the loss with respect to H can be expressed as a sum of per-example gradients, we compute its gradient for the samples residing on each GPU. Then a single all-reduce step is needed to aggregate the gradients for all of the examples. Then each GPU applies the gradient descent step to their own local copies of H.

#### **D.4. Other Considerations**

We initialized W using the uniform distribution on [0,1]. We initialized H using a normal distribution with zero mean and standard deviation of  $\sqrt{2}/\sqrt{Cn}$ . Since the PEFs were normalized to unit Frobenius norms, we chose this scaling so that the initial reconstructions would also have roughly unit Frobenius norms as well.

After initialization, we found it crucial to freeze W and only train H for a bit before commencing joint training. This is because if the H is a poor fit for the W, the W update step will end up setting W to zero. Since the W update is multiplicative, it remains zero throughout the remainder of training if this happens. We suspect that this behavior can be explained due to the nature of the multiplicative update step. It can be shown that the multiplicative update step is equivalent to gradient descent with a variable element-wise learning rate (Burred, 2014). Unlike traditional gradient descent that uses a small gradient step, the variable learning can become large. This makes it possible for the W to jump directly to zero or some similarly small value. If the loss is greater than the Frobenius norm of the PEFs, then setting W to zero will result in a lower loss. Hence, jumping to zero can decrease the loss in such cases.

## **D.5.** Convergence

While we do not provide a proof of convergence of our NPEFF decomposition algorithm, we can make a heuristic argument for its convergence. Following the proof of convergence for regular multiplicative-update NMF (Lee & Seung, 1999), we can show that the loss will be non-increasing following the W-update step. For a sufficiently small step size, we can expect the gradient descent step from the H-update to not increase the loss as well. Since the loss is bounded from below by 0, it follows that the loss should eventually converge. When actually running NPEFF, we found the loss to be non-increasing with the rate of decrease decelerating as the number of steps increased.

## D.6. Decomposition on Randomly Projected PEFs

Let us see consider the difference between an update step in the original and non-projected set-ups. Let  $A \in \mathbb{R}^{n \times p}$  denote the random projection matrix used. While random projections only approximately preserve inner products, i.e.  $AA^T \approx I$ , we will make that assumption that they preserve inner products exactly, i.e.  $AA^T = I$ , to show that our algorithm commutes with random projections under that assumption. Let  $G_i' = G_i A$  and H' = HA denote the projected PEFs and pseudo-Fisher matrices, respectively. Note that the random projection will not directly affect the coefficients W.

Let's first look at the W-update step. Computing the rank-3 tensor B is equivalent to computing  $G_iH^T$  for  $i=1,\ldots,m$ . We have  $G_i'H^T=G_iAA^TH^T=G_iH^T$ , so B is left unchanged when using the projections. The numerator N is purely a function of B, so it is unchanged as well. The denominator D depends on projected quantities solely through  $HH^T$ . Since  $H'H'^T=HAA^TH^T=HH^T$ , the denominator is unaffected by the use of the projection. Since both N,D are unaffected by the projection, the W-update step is the same regardless of whether we using random projections.

Now let's look at the H-update step. Since we have shown that  $H'H'^T = HH^T$ , it follows that  $T_1' = T_1A$ . Similarly since the random projection does not affect B, we can show that  $T_2' = T_2A$ . Let  $\eta > 0$  denote the learning rate used in the H-update step. Originally, the H-update step proceeds as  $H \mapsto H - \eta(T_1 + T_2)$ . With the random projection, the updated H' is provided by  $H' - \eta(T_1' + T_2') = (H - \eta(T_1 + T_2))A$ . Essentially, we have shown that the H-update step commutes with random projections; performing an H-update in the original space followed by a random projection is equivalent to performing the projections first followed by the update step on the projections.

We have just shown that both the W-update and H-update leave the relationship between original and projected quantities unchanged: W' = W and H' = HA. Thus by induction, these relationships hold after an arbitrary number of update steps. Hence operating on projected PEFs will produce the same coefficients as operating on original PEFs. Furthermore, the final pseudo-Fisher vectors from the projected decomposition will be equal to the projections of the final pseudo-Fisher vectors from the original decomposition.

One major caveat of this analysis, however, is that it assumes that the random projections preserve inner products exactly. In reality, inner products are only approximately preserved by the projections. Hence this analysis should only be expected to hold approximately in practice.

## E. Task Formulations

#### **E.1. SST2**

SST2 consists of sentiment analysis of a sentence. Given a sentence, we construct a prompt via the template Review:  $\{\text{sentence}\}\setminus \text{nSentiment}:$ . The labels used for this task are Negative and Positive. To get a distribution  $p'_{\theta}(y|\mathbf{x})$  over two labels, we start with the full model distribution  $p_{\theta}(y|\mathbf{x})$  over the entire vocabulary given the context. We look at the first token in the tokenization of each label labels and obtain their corresponding probabilities from  $p_{\theta}(y|\mathbf{x})$ . These two probabilities are then normalized to get a distribution  $p'_{\theta}(y|\mathbf{x})$  over the labels. As a practical note, we can obtain the logits of  $p'_{\theta}(y|\mathbf{x})$  by simply selecting the logits corresponding to label tokens from  $p_{\theta}(y|\mathbf{x})$  due to properties of the softmax function.

## E.2. TriviaQA

TriviaQA is an open-form question answering task where the model generates an answer given a question. Given the question, we construct a prompt via the template Question: {question}\nAnswer:. We take  $p_{\theta}(y|\mathbf{x})$  to be the model's next-token predictive distribution given this context.

## F. Perturbation Experimental Details

Compressed sensing aims to solve the constrained optimization problem

$$\min_{\mathbf{x}} \left\{ \|\mathbf{x}\|_1 : A\mathbf{x} = \mathbf{b} \right\},\tag{5}$$

where  $\mathbf{x} \in \mathbb{R}^n$  is the reconstruction which we wish to find,  $\mathbf{b} \in \mathbb{R}^p$  is the projected vector, and  $A \in \mathbb{R}^{p \times n}$  is the random projection matrix. However, we use the unconstrained relaxation

$$\min_{\mathbf{x}} \|\mathbf{x}\|_1 + \frac{1}{2\mu} \|A\mathbf{x} - \mathbf{f}\|_2^2, \tag{6}$$

where  $\mu > 0$  is a hyperparameter controlling sparsity of the solution.

We used the fixed point continuation (FPC) solver from Hale et al. (2007) to solve (6) since it only requires matrix-vector products with the random projection matrix and its transpose. This is a good fit for our custom CUDA kernels implementing the random projections. We use the default hyperparameter values of  $\gamma=0.99,\,\beta=4$ , and equation (73) from Hale et al. (2007) to set  $\tau$ . We used a value of 4e-5 for the hyperparameter  $\mu$ . We also use a single inner iteration since we found that to produce the best results in our perturbation experiments. We found this algorithm to produce reconstructions quickly, typically taking at most a few seconds.

<sup>&</sup>lt;sup>1</sup>The SmolLM2 tokenizer prepends the space to the start of tokens, so our labels technically have a space at the start.

Table 7. Percentage of matching components from NPEFF decomposition 2 with the same tuning as their match from NPEFF decomposition 1 for SNLI.

NPEFF Comps 1	NPEFF Comps 2	PERCENT OF TUNED MATCHES
2048	8192	87.5
512	8192	84.8
128	8192	82.8
512	2048	89.2
128	2048	87.1
128	512	90.3

Table 8. Percentage of matching components from NPEFF decomposition 2 with the same tuning as their match from NPEFF decomposition 1 for SST2.

NPEFF Comps 1	NPEFF Comps 2	PERCENT OF TUNED MATCHES
32	64	82.1
32	128	72.7
32	256	74.0
32	512	76.8
64	128	66.7
64	256	71.1
64	512	71.2
128	256	82.6
128	512	81.2
256	512	82.3

## G. Number of Components Ablation Full Breakdown

A breakdown of fraction of matching components for NPEFF decompositions with preserved tunings with varying number of components is provided in Table 7 for SNLI and Table 8 for SST2.

#### H. SAE Additional Information

## H.1. Training Details

As is common practice, we constrain rows of the encoder and columns of the decoder to have unit L2 norm, which causes these parameters to lie on a manifold. Like Bricken et al. (2023), we project gradients onto the tangent space of this manifold before passing them to Adam. Following Gao et al. (2024), we initialize the decoder to the transpose of the encoder. We did not do anything else to mitigate the issue of "dead" latents during training since this was not a major issue for us. We normalized per-token activations to unit L2 norm before passing them to the SAE. We also did this when computing top examples for each SAE component. In all of our experiments, we used a learning rate of 1e-3. We used a batch size of 4096 activations and trained for 51,200 batches.

#### **H.2. SAE Tunings**

Full breakdowns for the tunings of SAEs are provided in Table 9 for k = 16, Table 10 for k = 32, Table 11 for k = 64, and Table 12 for k = 128.

## I. Unlearning

## I.1. Unlearning Method

Our unlearning method can be seen as a modified version of Yao et al. (2023). Our examples to forget belong to a forget set  $\mathcal{D}_f$  with rest of the examples being put into the retain set  $\mathcal{D}_r$ . The loss to optimize can be decomposed into a loss over the forget set and retain set:  $\mathcal{L} = \epsilon_f \mathcal{L}_f - \epsilon_f \mathcal{L}_f$ , where  $\epsilon_f, \epsilon_r > 0$  are hyperparameters controlling the trade-off between unlearning the forget set and retaining performance on the other examples. Since the forget loss  $\mathcal{L}_f$  has a multiplier of -1 in

Table 9. Breakdown of SAE component tunings for SNLI with k = 16.

	Non-Dead Comps			PREDICTION TUNED		TOKEN TUNED	
LAYER	Count	Count	%	Count	%	Count	%
2	5479	13	0.24	10	0.18	2008	36.6
5	5845	55	0.94	34	0.58	2097	35.0
8	5990	135	2.25	153	2.55	1344	22.4
11	5597	220	3.93	278	4.97	393	7.02

Table 10. Breakdown of SAE component tunings for SNLI with k=32.

Layer	NON-DEAD COMPS COUNT	LABEL T COUNT	UNED %	PREDICTI COUNT	ON TUNED %	TOKEN T COUNT	TUNED %
2	7260	12	0.17	13	0.18	2597	35.8
5	7652	70	0.91	46	0.60	2809	36.7
8	7939	171	2.15	190	2.39	1790	22.5
11	7865	274	3.48	390	4.96	587	7.46

the full loss, minimizing the full loss  $\mathcal{L}$  tries in part to maximize the forget loss  $\mathcal{L}_f$ .

Unlike Yao et al. (2023), we do not include a "mismatch" loss term. Since we are focused on our TriviaQA set-up, we only look at the model's next token prediction  $p_{\theta}(y|\mathbf{x})$  given the question context  $\mathbf{x}$ . Thus instead of running gradient ascent using a labeled cross entropy loss on the forget set, we run gradient ascent on the KL-divergence between the unlearned and original model's predictions on the forget set. Thus we have

$$\mathcal{L}_f = \frac{1}{|\mathcal{D}_f|} \sum_{\mathbf{x} \in \mathcal{D}_f} D_{\mathrm{KL}} \left( p_{\theta}(y|\mathbf{x}) || p_{\theta_{\mathrm{og}}}(y|\mathbf{x}) \right), \tag{7}$$

where  $\theta$  denotes the parameters of the unlearned model and  $\theta_{og}$  denotes the frozen parameters of the original model. Our retain set is the same as Yao et al. (2023):

$$\mathcal{L}_r = \frac{1}{|\mathcal{D}_r|} \sum_{\mathbf{x} \in \mathcal{D}_r} D_{\mathrm{KL}} \left( p_{\theta_{\mathrm{og}}} || p_{\theta}(y|\mathbf{x}) \right), \tag{8}$$

where we use the forward KL instead of the reverse KL. In practice, we optimize  $\mathcal{L}$  by sampling a mini-batch from  $\mathcal{D}_f$  and  $\mathcal{D}_r$  and then computing  $\mathcal{L}_f$  and  $\mathcal{L}_r$  restricted to that mini-batch.

## I.2. Unlearning Experimental Details

We used the Adam optimizer with a learning rate of 1e-4. Since our forget set always has a single example, we use a batch size of 1 for the forget example. For the retain set, we sample 32 examples at random and then concatenate the fixed set of 12 examples to it. Recall those 12 examples either belong to an NPEFF component's top examples in mitigation experiments or are random examples in the control experiments. We use an  $\epsilon_f$  of 1e-1 and  $\epsilon_r$  of 1e1. We train for 75 batches.

## J. Component Top Examples

Top examples of random components are presented in Figure 3 for SNLI, in Figure 4 for SST2, and Figure 5 for TriviaQA.

Table 11. Breakdown of SAE component tunings for SNLI with k=64.

	NON-DEAD COMPS			PREDICTION TUNED		TOKEN TUNED	
LAYER	Count	Count	%	Count	%	Count	%
2	8188	29	0.35	19	0.23	4072	49.7
5	8187	98	1.20	79	0.96	3729	45.5
8	8186	184	2.25	203	2.48	1731	21.1
11	8184	296	3.62	407	4.97	507	6.20

Table 12. Breakdown of SAE component tunings for SNLI with k=128.

T	NON-DEAD COMPS	LABEL T			ON TUNED	TOKEN 7	
LAYER	Count	Count	%	Count	%	Count	<u>%</u>
2	8191	22	0.27	17	0.21	3542	43.2
5	8183	78	0.95	55	0.67	3528	43.1
8	8191	173	2.11	202	2.47	1957	23.9
11	8188	308	3.76	390	4.76	844	10.3

#### Component 1

[P] A man and woman pose for a picture together, with neither smiling.

[H] People are posing

[P] A woman and girl pose for picture with a man in a space suit.

[H] People are posing for pictures

[P] A woman and man are posing for a picture against a pink wall.

[H] People are posing

[P] Two men and a woman pose for a picture.

[H] People are posing.

[P] A female and male embrace in front of a sculpture.

[H] People are embracing

#### Component 2

[P] A man in a blue shirt with a duffel bag and a woman in a yellow jacket pushing a baby

[H] The man is swimming in a pool.

[P] A man with dark hair is wearing a white shirt with printed flames and is holding a Component 7 pair of tongs

[H] A man is swimming in a pool.

[P] A young boy wearing a white tunic, white pants, and a yellow belt is standing on [P] A person biking down a city street in gloves and a warm hat. his left leg

[H] A boy is swimming in a pool.

[P] A man in a black shirt is looking at a woman in a white shirt with a silly face.

[H] A man is swimming in a swimming pool.

 $[P]\ A\ woman\ in\ jeans\ and\ a\ red\ coat\ and\ carrying\ a\ multicolored\ handbag\ spreads\ put\ [H]\ A\ man\ is\ shovelling\ snow.$ her arms while

[H] A woman is swimming in a pool.

### Component 3

[P] A man walking past a bench, with a yellow curb.

[H] The man is moving.

[P] A man walks past blue payphones.

[H] The man is moving.

[P] A woman in a long white dress and white boots is walking along a stone structure [H] A person is surfing in a competition. with white stone columns.

[H] The woman is moving.

[P] Guy walking his bicycle through a tunnel.

[H] The guy is moving.

[P] Three men walking in front of a colorful tent with a sign on it.

[H] The men are moving.

## Component 4

[P] Three dogs play near the water.

[H] Dogs are playing near water.

[P] Three dogs run on beach, two playing with unknown object.

[H] Dogs are running on the beach.

[P] Two dogs run in the snow; one has a ball.

[H] Dogs are running in the snow.

[P] Two dogs play in the snow.

[H] Dogs are playing in the snow.

[P] Three dogs run through water and grass.

[H] Dogs are running on the grass.

Component 5 [P] A man is kneeling down with a child on a beach where bright blue [H] The dog is going somewhere. and red boats are stationed in the background

[H] A man and boy are outside.

[P] A child is riding a unicycle along a riverside path next to a woman who is walking a [H] The man is dancing in the rain in a field.

[H] A child and a woman are outside.

[P] A man and woman walking across a street next to a mural of a man giving a woman a golden apple

[H] A man and a woman are outside.

[P] A girl wearing a pink hat is walking beside a sheep on a dusty path.

[H] A girl and sheep are outside

[P] A man walking by a woman who is standing on the street smoking a cigarette.

[H] The man and woman are outside.

#### Component 6

[P] A crowd of people stand in the background of a set of tables draped in white with various used toys

[H] A crowd of people stand in the background.

[P] A group of kids walk down an urban street passing by graffiti and a small car and a

[H] A group of kids walking down the street.

[P] A group of people looks out over a railing that is set on a glass wall making their legs visible

[H] A group of people look over a railing.

[P] A group of people standing on a hillside decorated with yellow flowers as fog rolls over a nearby mountainside

[H] A group of people stand on a hillside.

[P] A group of people enter a doorway next to a red sign reading "welcome bikers".

[H] A group of people enter a doorway.

[P] A man holding a flag stands next to a woman wearing black and white.

[H] The man is shoveling snow

[H] A person shovels snow.

[P] An elderly man stands on a ladder tending the leaves of a tree.

[H] An elderly man is shoveling snow

[P] A man wearing a santa hat is playing a musical instrument.

[P] A man in a green vest and clothing sweeps up trash on the sidewalk underneath the shade of a tree.

[H] The man is shoveling snow.

#### Component 8

[P] A person, crouching on a surfboard, is surfing in a body of water.

[H] A person is surfing in a competition.

[P] A person surfing in the distance with the wave collapsing just behind him.

[P] A man catching a wave on a surfboard being observed or photographed by others from the shore.

[H] The man is in a surfing competition.

[P] The man is snowboarding down a snowy hill.

[H] The man is in a competition.

[P] A four wheel drive car is driving through the mud. [H] The four wheel drive car is in a competition.

#### Component 9

[P] A woman jogs down the rode near a rocky shore.

[H] The woman is going for a run.

[P] A person jogs down a paved surface in a rural setting.

[H] The person is going for a run.

[P] A dog jumps for the woman's treat.

[H] The dog is doing a trick.

[P] A man hurls a ball down his lane at a bowling alley.

[H] The man is keeping score.

[P] A dog leaps out of the water.

## Component 10

[P] A bearded man wearing a black cap, a black short - sleeve shirt, and blue pants

[P] A man in black and white cap and scarf.

[H] A man is going swimming at a public pool.

[P] Men in orange vests and hard hats.

[H] A group of children on a playground.

[P] A dark - haired woman wearing a brown jacket and fatigue bottoms and a bald

[H] A man and a woman standing on the beach discuss the best place to

[P] An older woman wearing a brown hat, a plaid shirt, and striped white pants

[H] A woman is taking the subway to go on a shopping trip.

Figure 3. Top examples of random components from NPEFF decompositions for SNLI in Section 3.1. The [P] denotes the premise and the [H] denotes the hypothesis.

Component 6

#### "nicholas nickleby" is a perfect family film to take everyone to since there 's no new " a christmas carol" out in the theaters this year. it 's not a motion picture; it 's a heck of a ride is a more fascinating look at the future than "bladerunner" and one of the most high-concept sci fi adventures attempted for the screen . it 's not half-bad the basic plot of "lilo" could have been pulled from a tear-stained vintage shirley it 's funny . it 's not too much of anything. downright transparent is the script 's endless assault of embarrassingly ham-fisted sex Component 2 jokes that reek of a script rewrite designed to garner the film a "cooler" pg-13 rating. reached its expiration date viewers will wish there had been more of the "queen" and less of the "damned." skip this dreck, rent animal house Component 7 stop buying tickets resonance donovan ... squanders his main asset rocks an all-time low for kevin costner drains Component 3 waste an engrossing and infectiously enthusiastic documentary . sewage a marvel of production design. Component 8 an unexpectedly sweet story of sisterhood. murder an extraordinary dramatic experience . murderer deliver a riveting and surprisingly romantic ride . crime Component 4 suicide bang-bang, shoot-em-up scene horror chatty fish Component 9 soap-opera a very ambitious project car-wreck a feature debut purr a powerful entity Component 5 a successful example the word - mindless , lifeless , meandering , loud , painful , obnoxious a powerful sequel of the word - mindless, lifeless, meandering, loud, painful, obnoxious Component 10 a zombie movie in every sense of the word - mindless, lifeless, meandering, loud, smart and fun painful, obnoxious smart comedy what the audience feels is exhaustion, from watching a movie that is dark (dark green smart movie , to be exact ) , sour , bloody and mean . smart, be low , very low , very very low , for the masquerade to work

Component 1

Figure 4. Top examples of random components from NPEFF decompositions for SST2 in Section 3.1.

#### Component 1

In Judaism, what is a 'Kever'?

In heraldry, what is a wyvern?

What is a Stiffkey (or Stewkey) Blue?

In CB jargon what is a bone box?

What is a 'tercel' ('tiercel' in the USA)?

#### Component 2

For her performance in which film did Meryl Streep win the Best Actress 'Oscar' earlier this year?

For her performance in which film did Meryl Streep win the Best Actress 'Oscar' earlier this year?

For his role in which film did Al Pacino win the Oscar for best actor in 1992? For her role in which film did Jane Darwell win the 'Oscar' for Best Supporting Actress in 1940 when aged 61?

For his role in which film did Al Pacino win the Oscar for best actor in 1992?

#### Component 3

"The names of how many US states begin with ""New""?"

"The names of how many US states begin with ""M""?"

"The names of how many US states begin with the letter ""I""?"

"The names of how many US states begin with ""New""?"

"The names of how many US states begin with ""M""?"

#### Component 4

Which famous actor was born in Beirut in 1964?

Which theatre critic devised and produced the erotic revue 'Oh! Calcutta!' in 1969?

Which poet died of septicaemia in the Aegean Sea in 1915?

Which theatre critic devised and produced the erotic revue 'Oh! Calcutta!' in 1969?

Which famous author spent 5 years in the 1920's as a police officer in Burma?

#### Component 5

A rat can survive longer without water than a camel?

A rat can survive longer without water than a camel?

A Wayzgoose is an annual outing or party in which industry?

A system known as SCOOT (Split Cycle Offset Optimisation Technique) is used to control our travel movements in what way?

A Sugar anniversary celebrates how many years of marriage?

#### Component 6

Which film tells of the exploits of singer Deco Duffe?

Which film tells of the exploits of singer Deco Duffe?

Which sitcom with Vickie Lawrence was a spin-off from the Carol Burnett Show?

Which sitcom with Vickie Lawrence was a spin-off from the Carol Burnett Show?

Which show was based on the autobiography of Gypsy Rose Lee?

#### Component 6

Who was Henry VIII's third wife?

Who was Henry VIII's third wife?

British monarch Henry VIII married which of his wives in 1540?

British monarch Henry VIII married which of his wives in 1540?

Which of Henry VIII's wives was the mother of Mary I?

#### Component 7

"Which product was advertised on TV with the slogan ""Good to the last drop""?"

"Which product was advertised with the slogan ""Good to the last drop""?"

"Which product was advertised with the slogan, ""Forces grey out, forces white in'"?"
"Which famous product was advertised on TV with the words ""Cleans and polishes in one on """

"Which famous product was advertised on TV with the words ""it won't let you down""?"

#### Component 8

How many apprentice boys shut the gates of Derry in December 1688 leading to the siege of the city?

How many theses did Martin Luther post on the door of the Castle Church of Wittenberg in October 1517?

How many Victoria Crosses were won at Rorke's Drift in 1879?

How many theses were nailed to a church door by Martin Luther in 1517 (generally accepted to be the Castle Church in Wittenberg, Germany, on All Saints Eve, 31 October)?

How many prisoners were locked in the Bastille in Paris when it was stormed by the people in 1789?

#### Component 9

Which Shakespeare play is mainly set in a forest outside Athens?

Which Shakespeare play is set in Illyria?

Which Shakespeare play is mainly set in a forest outside Athens?

Which Shakespeare play has the siege of Troy as its setting?

Which Shakespeare play has the siege of Troy as its setting?

#### Component 1

Which gas forms 80% of Earth's atmosphere?

Which gas forms approximately 1% of the atmosphere?

Which gas forms approximately 1% of the atmosphere?

Which gas forms approximately 1% of the atmosphere?

Which gas forms about 78% of the Earth's atmosphere?

Figure 5. Top examples of random components from NPEFF decompositions for TriviaQA in Section 3.1.